Opto-Electronics Review

journal homepage: https://journals.pan.pl/opelre

Chen chaotic system-based wideband metamaterial absorber

Mehmet Bakır[1*], Ahmet S. Köksal[1], Mertcan Oral[1], Muharrem Karaaslan[2,3], Berker Çolak[2], Ugur C. Hasar[4], Arlet P. Franco[5], Fikret A. Teksen[2]

[1] Department of Computer Engineering, Bozok University, Yozgat, Turkey
[2] Department of Electrical and Electronics Engineering, Iskenderun Technical University, Iskenderun, Hatay, Turkey
[3] ISTE Center for Science and Technology Studies and Research (ISTE-CSTSR), Iskenderun, Hatay, Turkey
[4] Department of Electrical and Electronics Engineering, Gaziantep University, Gaziantep, Turkey
[5] Grupo de Investigación Ingeniar, Facultad de Ciencias Básicas e Ingenierías, Corporación Universitaria Remington, Calle 51 #51-27, Medellín, Colombia

Article info

Article history:
Received 12 Sep. 2024
Received in revised form 05 Feb. 2025
Accepted 22 Feb. 2025
Available on-line 18 Mar. 2025

Keywords:
Magtrex 555;
pattern generation;
Chen attractor;
metamaterial absorber.

Abstract

This manuscript introduces a novel wideband metamaterial absorber targeting the 2 GHz to 20 GHz range. The design employs a chaos theory, specifically the Chen attractor system, to generate fractal-structured patterns that enhance electromagnetic absorption. These patterns exhibit multi-resonant behaviour, providing superior efficiency compared to conventional periodic designs. The absorber is further optimized with a Magtrex 555 substrate (0.51 mm thick), known for its frequency-dependent permittivity and permeability, which amplifies performance. This combination of chaotic structures and optimized substrate achieves over 90% absorption efficiency across a broad frequency range. Comprehensive simulations and parametric studies validate the absorber effectiveness, significantly improving bandwidth and absorption capacity. The design is well-suited for electromagnetic shielding, energy harvesting, and stealth technology applications. Future works will emphasize real-world performance testing to validate practical applications in wireless communication, sensing technologies, and defence. By combining chaotic dynamics with substrate optimization, this work contributes significantly to next-generation electromagnetic absorbers, offering enhanced broadband absorption for various applications.

1. Introduction

Metamaterials are artificial electromagnetic materials with negative refractive index and permeability [1, 2]. Metamaterials are widely used in microwave absorbers, sensors, polarization converters, and Lense technologies [3–6]. Microwave metamaterial absorbers (MAs) are specifically designed to absorb electromagnetic waves within certain frequency bands. This absorption can be used across a wide range of applications in military stealth to reduce radar cross-section, electromagnetic combability, energy harvesting systems and sensing applications [7–10].

The absorption frequency of MAs is generally determined by patch patterns, which may consist of regular shapes such as split-ring resonators or chaos-based patterns [11–13]. Broadband MA design is challenging, especially between 2 and 20 GHz. To achieve broadband absorption, some researchers designed pyramid-shaped absorbers [14–17], while others developed periodically arranged elements [18–20] to extend the bandwidth [21, 22].

In recent years, the field of MA design has employed chaotic structures driven by the need for more efficient and adaptable technologies across various applications, as follows. The development of wideband ground-backed complementary split-ring resonator (WG-CSRR) arrays has proven to be a significant advancement. These arrays, operating at a resonance frequency of 5.6 GHz, exhibit a half-power bandwidth (HPBW) of 44% [23]. Another study presents a novel method to design electromagnetic stealth metasurfaces that conform to arbitrary non-uniform rational B-spline (NURBS) curved surfaces. These metasurfaces introduce an innovative approach to design electromagnetic stealth metasurfaces that conform to arbitrary NURBS curved surfaces. The use of chaotic

*Corresponding author at: mehmet.bakir@bozok.edu.tr

https://doi.org/10.24425/opelre.2025.154199
1896-3757/ Association of Polish Electrical Engineers (SEP) and Polish Academic of Sciences (PAS). Published by PAS

projection mapping achieved a 5 GHz absorption within the range of 36 GHz–41 GHz [24]. Applying chaotic dynamics in electromagnetic wave propagation demonstrates significant potential to improve wave control. Focusing on the microwave frequency range, particularly around 1–10 GHz, this approach allows for more precise manipulation of wave propagation, which could lead to advancements in antenna design and waveguides by using chaos [25]. Another study uses the Rossler chaos model to explore designing and developing a wideband, high-absorption electromagnetic absorber using a chaos-patterned metasurface. The proposed metasurface performs better in achieving low reflectivity over a broad frequency range, making it suitable for applications in anechoic chambers and other electromagnetic wave absorbers. Numerical simulations and experimental results confirm that the chaotic surface patterns enhance absorption by providing complex edge structures and strong coupling effects, resulting in a significantly broader bandwidth than conventional absorbers. This approach offers a novel method for improving electromagnetic absorption through the use of fractal-structured patterns in metasurfaces [26].

In this work, a chaos theory was employed to develop structures that operate between 2 GHz and 20 GHz during the design and application part. The Chen attractor, a prominent chaotic system governed by three nonlinear differential equations, plays a pivotal role in this process. Its complex dynamics makes it an ideal candidate for creating chaos-based patterns that can be embedded into metamaterials [27]. These patterns enhanced wave absorption and scattering across a broad frequency spectrum. The unpredictable patterns generated by the Chen attractor have been used as a metamaterial to interact with electromagnetic waves in a highly complex manner, which is particularly beneficial for the proposed work [28, 29]. By adjusting the parameters within the Chen attractor equations, the proposed work can control the chaotic dynamics to optimize the metamaterial performance between 2 GHz and 20 GHz. The proposed study distinguishes itself from similar works by achieving over 90% signal absorption in the 2–20 GHz frequency range. This success is attributed to the use of the Chen attractor and the innovative aspect of the research lies in exploring the relationships between chaotic parameters and their effects on signal absorption. The ability to correlate these chaotic dynamics with enhanced electromagnetic properties underscores the novelty of this approach.

2. Materials and methods

This study used patterns derived from the Chen chaotic system for a broadband metamaterial absorber design. The methodological process consists of five main stages, as shown in Fig. 1. First, the Chen chaotic system initial conditions and parameter values were determined meticulously. These parameters play a fundamental role in the creation of chaos-based patterns. In the second stage, these patterns were generated using the determined initial conditions and parameters. These patterns serve as essential building blocks for the metamaterial design.

In the third stage, the generated patterns were integrated into a design of the metamaterial structure. This stage optimized the integration of the patterns to the surface and

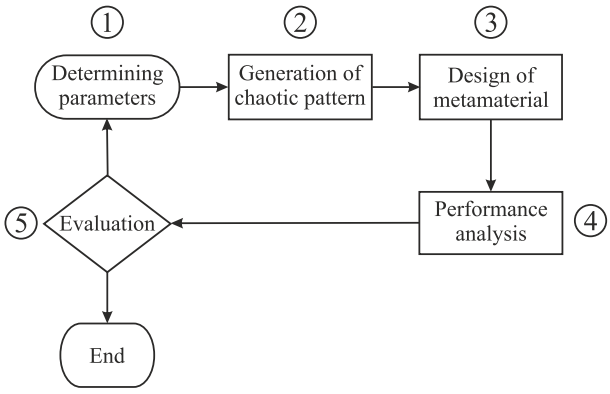

Fig. 1. Diagram shows the main stages of the methodological process.

electromagnetic properties of the metamaterial. In the fourth stage, the electromagnetic wave absorption performance of the designed metamaterial was analysed in the frequency range of 2–20 GHz. This analysis evaluated the effectiveness of the design and whether an expected performance criterion of 90% absorption was achieved.

Finally, in the fifth stage, if the absorption performance is above 90% according to the performance analysis results, the process is completed, and the results are disseminated. If the performance remains below 90%, it is returned to the first stage, and parameter adjustments continue until optimal results are achieved. Each stage of this methodological process is explained in detail in the following sections.

2.1. Chen chaotic system and pattern generation

The Chen chaotic system consists of three simultaneous nonlinear differential equations widely used in studying dynamical systems. This system exhibits chaotic behaviour and is an ideal tool for generating complex and unpredictable patterns for design utilization. Its purpose to be used in metamaterial design is to generate geometrically optimized patterns to create surface resonators that provide broadband absorption. Combined with the Julia set algorithm, this system enables the modelling of chaotic dynamics as a physical structure. The equations of the Chen system are defined as follows:

$$\dot{x} = a(y - x), \tag{1}$$

$$\dot{y} = (c - a)x - xz + cy, \tag{2}$$

$$\dot{z} = xy - bz, \tag{3}$$

where x, y, and z are the state variables of the system, representing quantities that change over time. The parameters a, b, and c determine the dynamics of the chaotic system. $\dot{x}$, $\dot{y}$ and $\dot{z}$ are the derivatives of these variables with respect to time and express the rate of change of the system.

The process from this system solution to the conversion of the obtained patterns into vector format and their use in metamaterial design is presented in detail below. The process includes the steps of creating time series from the Chen attractor, visualizing with the Julia set algorithm, Gaussian filtering, binary transformation, small area cleaning, and conversion to vector geometries.

Firstly, the Chen chaotic system is solved numerically using the Euler method. In this method, the step interval has been determined as $h = 0.014$. The initial conditions for the system are fixed as $x = 5$, $y = 5$, and $z = 5$. The parameters b and c have been assigned as 3 and 22, respectively. The parameter a is changed in a certain range to generate different patterns. As a result of this step, a time series that provides information about the dynamics of the Chen system evolution over time has been obtained.

Then, these obtained time series are normalized and scaled by a certain coefficient. This process ensured the rescaling of the time series within a specified range. Mathematically, this process can be expressed as follows:

$$[x, y, z] = K \times Norm([x, y, z]), \tag{4}$$

where *Norm* represents the normalized form of the x, y, and z time series, and K is the coefficient defined as 8.

Using the x and y values in these scaled time series, the ω complex number $\omega = x + iy$ is created. These ω values are given as input to the Julia set function. The Julia set is a fractal structure obtained by an iterative process in the complex plane [30] and is a highly effective method for visualizing data obtained from chaotic systems [31]. The following equation defines the Julia set:

$$\omega_{n+1} = \omega_n^2 + d, \tag{5}$$

where ω_n represents the complex number obtained in the previous iteration for the Julia set, d is the constant complex number and is determined as $-0.175 + 0.655i$ in this study, and ω_{n+1} is the new complex number to be obtained in the next iteration.

For each x and y pair, 100 iterations have been performed on the Julia set. During these iterations, the process is terminated when the magnitude of the values produced by the function exceed a predefined escape value ($\omega > /K + d/$). This escape value has been established to prevent the function outputs from diverging to infinity.

The number of iterations determines the pixel colour property of the image to be created. To create a 480×480 pixel image, $480 \cdot 480 = 230\,400$ input data (time series) were generated using the Chen system. Thus, colour values are calculated for all pixels of the image. As a result, a fractal image of 480×480 pixels has been created.

In the next step, the image created with the Julia set algorithm is filtered through a Gaussian filter to soften the edges. The Gaussian filter allows for a smoother and more homogeneous structure by softening the sharp edges and roughness in the image [32]. This is important for optimizing the electromagnetic wave absorption by providing smoother transitions on the surface of the design. In this process, the filter is set to a standard deviation value of 4 on both the horizontal and vertical axes.

The pattern obtained by Gaussian filter is converted to a binary form using a certain threshold value after the edge smoothing process. In this transformation, the threshold value is selected as 1 and only pixels with the maximum brightness are defined as white (1) and all other pixels are defined as black (0). This process allows simplification of unnecessary details in the surface patterns to increase electromagnetic performance.

In the next step, small areas in the image are cleaned. First, all white areas consisting of neighbouring pixels and having a total area smaller than 128 pixels have been removed. Then, the same process is applied to small black areas. These processes help achieve a clearer and more distinct structure by cleaning unnecessary small areas in the image.

In the final step, the binary image obtained and processed in the previous steps is converted to a vector format for the metamaterial design. The conversion of the patterns obtained by the Julia set algorithm from binary to vector format has been implemented to optimize the electromagnetic absorption performance of the surface resonators. The vector format provides a scale-free structure of the surface geometry and allows the design to be scaled in different dimensions. These geometries, modelled as metallic patches in the CST Studio Suite software, reflect the resonance properties of the chaotic system onto a physical surface, creating multiple resonance effects in a wide frequency range. This process is a critical step in the conversion of the patterns obtained from the Chen attractor into a physical structure in metamaterial design.

The Chen system exhibits chaotic behaviour for certain values of the parameters a, b, c and initial conditions of x_0, y_0, z_0. The range of these values is available in the studies such as in [33]. In this study, the values $a = 35$, $b = 3$, $c = 28$ and $x_0 = 0$, $y_0 = 0$, $z_0 = 0$, which are frequently used in the literature, have been initially selected and then new patterns have been produced by roughly changing these values. The designs realized with each new pattern have been tested. According to the test results, a baseline of $a = 35$, $b = 3$, $c = 22$ and $x_0 = 5$, $y_0 = 5$, $z_0 = 5$ has been determined. Later, in order to make finer tuning and further increase the absorption performance, optimization is performed by keeping all other parameters constant and only a parameter is altered. Here, the a parameter is used as the control parameter. The a parameter is modified with 0.5 step intervals between the values 15 and 40, where the system behaves chaotically. Figure 7(a) shows the shape of the patterns obtained for three different parameters. The best absorption performance is observed for $a = 35$. The phase space trajectories of the Chen system for this selected case are depicted in Fig. 2.

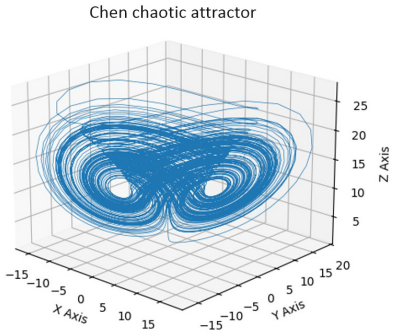

Fig. 2. Chen chaotic attractor in X, Y and Z space.

The patterns obtained from the chaotic system exhibit fractal characteristics, meaning that they are composed of self-similar structures at different scales. Fractal patterns, by definition, exhibit complexity and irregularity, with repeating elements that are not periodic but instead show scaling behaviour. The self-similarity of fractals implies

that although patterns repeat across scales, they do not follow a strict periodic rhythm like those seen in regular, periodic structures. Instead, their repetition is irregular, characteristic of chaotic systems where order arises within apparent disorder.

The authors analysed the Fourier amplitude spectra and radial profiles of the images obtained from these patterns to verify that these fractal patterns do not exhibit periodic structures. The analysis results for three different values of a are shown in Fig. 3. Upon examining the radial profile of the Fourier amplitude spectrum, it is seen that the profile decreases regularly from the zero frequency (centre). While the spectrum does not appear completely flat, as might be expected from a completely random pattern, it does not show clear repetitive peaks indicative of periodic structures. The Fourier amplitude spectrum indicates the presence of a concentration of energy in low frequencies, which is typical for patterns generated from chaotic systems. This suggests that large-scale intensity variations dominate the overall structure of the pattern.

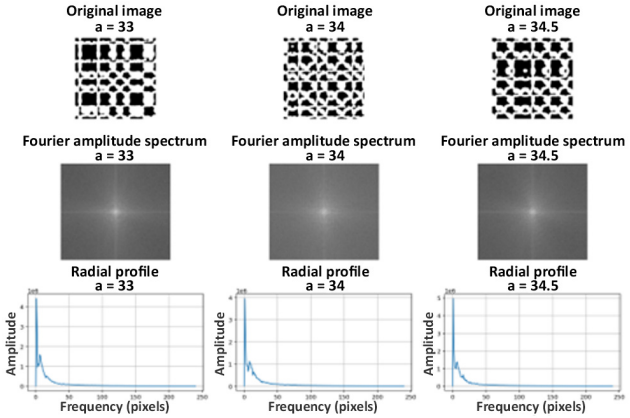

Fig. 3. Fourier analysis and radial profiles of the generated images.

The presence of slight structure in the Fourier spectrum, such as two peaks at low frequencies, suggests that some regularities or repeating elements may exist within the image. However, these peaks occur at irregular intervals, which indicates that the pattern does not exhibit strict periodicity. This irregularity aligns with the fractal nature of the image, where repetition is not uniform or periodic but instead scales in an unpredictable manner. Thus, while there are hints of repetition in the Fourier spectrum, the patterns themselves do not exhibit clear periodicity.

While not periodic, patterns derived from a chaotic mathematical system retain a form of deterministic structure that allows them to be recognized as chaotic but still organized in a non-periodic, fractal manner. This "order within chaos" is a hallmark of chaotic systems, where the underlying dynamics produce complex, non-periodic structures. The slight structure observed in the Fourier spectrum reflects this balance, where large-scale variations dominate, but finer details are irregular, as expected from fractal-like patterns.

3. Design and analysis

The nonlinearity in the Chen system is crucial for the onset of chaos. The quadratic components within the equations introduce the necessary complexity, ensuring that the system avoids converging into periodic or stable states. In this part of the study, the fractal-patterned image, which has been converted into vector form, is first imported into the microwave simulator. This software is employed to design the microwave absorber and to simulate its performance. The fractal pattern represents the resonator section of the design. As depicted in Fig. 4, the authors introduce a chaotic absorber design with specific parameters as shown in Fig. 4. Figure 4 seems to illustrate the layout of a chaotic absorber featuring copper patterns of varying sizes and configurations on a Magtrex 555 specialized microwave substrate material known for its frequency-dependent permittivity and permeability. This characteristic makes it ideal for high-frequency applications like antennas and microwave absorbers. Thickness of the dielectric layer is assigned as 0.51 mm to enable effective electromagnetic shielding and wave absorption. The back side of the dielectric material is coated with copper, preventing electromagnetic wave transmission. Boundary conditions are assigned as $E_t = 0$ and $H_t = 0$ throughout and Y directions, respectively, while it is open in Z directions.

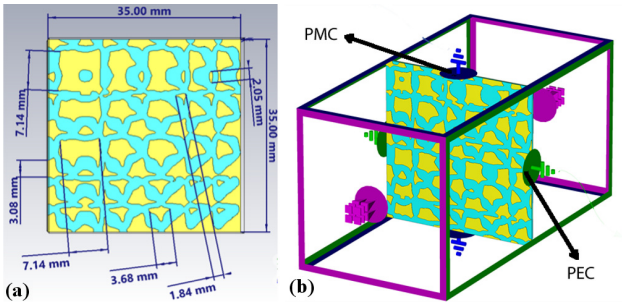

Fig. 4. (a) Dimensions of the proposed metamaterial absorber front side, (b) boundary conditions and profile view.

The width of the proposed structure is specially chosen to maximize bandwidth and absorption between 2 GHz and 20 GHz. To demonstrate the effect of the substrate width on absorption, the substrate width is increased between 20 mm and 35 mm with a step of 5 mm, and then simulation is repeated for these steps. According to the simulation results, the absorptivity is decreased after 12 GHz, as shown in Fig. 5, due to low interaction, which creates absorptivity in these frequencies.

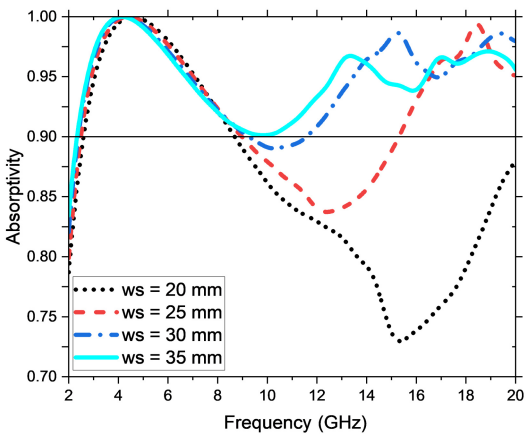

Fig. 5. The effect of substrate width which is adjusted between 20 mm and 35 mm on the absorption plot.

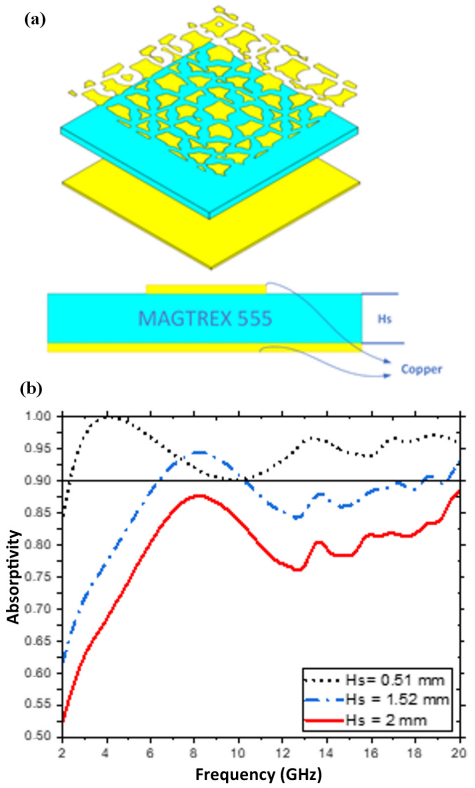

Fig. 6. Effect of substrate thickness on absorptivity: (a) profile view of the proposed structure, (b) absorption plot between 2 GHz and 20 GHz.

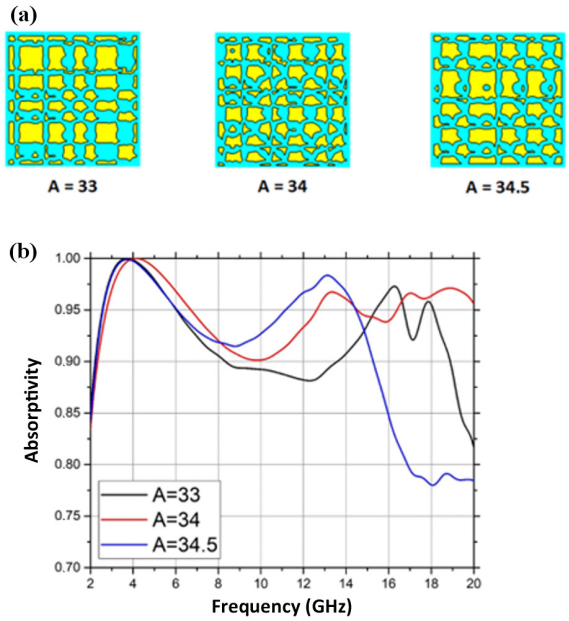

Fig. 7. A-parameter effect with the value of 33, 34, and 34.5: (a) top view of designed chaotic surfaces with these values, (b) simulated absorption plot by using these surfaces between 2 GHz and 20 GHz.

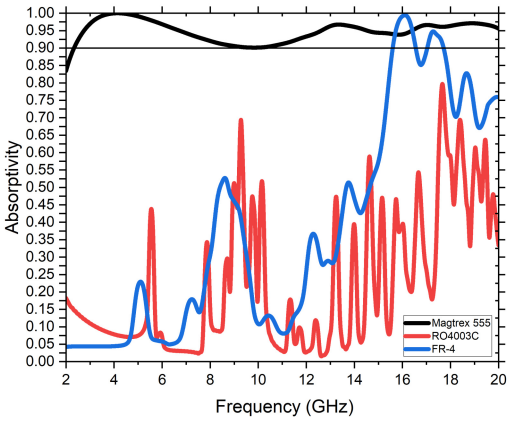

Fig. 8. Comparison of different substrates on absorptivity.

To show the effect of Salisbury screen on absorption, 0.51 mm, 1.52 mm, and 2 mm dielectric thicknesses have been simulated and the obtained results are presented in Fig. 6. Figure 6(a) presents the perspective and side views of the modelled chaotic system-based absorber structure. Figure 6(b) illustrates the impact of substrate thickness variations on absorptivity. As depicted, the absorption ranges change by 35% and 90% in the related frequency range. When it is set to 1.52 mm, the absorption value alters between 70% and 98% in the range. When the substrate thickness is set to 0.51 mm, the best absorption value has been observed between 85% and 90%. Low capacitance due to small thickness affects the overall resonance between 2 GHz and 20 GHz.

Furthermore, the chaotic control parameter "*a*" is examined to determine its impact on absorptivity. Figure 7(a) illustrates the chaotic control parameter effect on the geometry variation for the values of "*a*" set at 33, 34, and 34.5, respectively. As indicated in Fig. 7(b), the optimal operating parameter is 34 for the chaotic control parameter. Notably, the absorption decreases significantly from 95% to 77% beyond 20 GHz when "*a*" is set to 34.5. Since this parameter is related the chaos, an attempt was made to find the best value of the parameter in this part of the study. Several parameters have been simulated to obtain this value, and once the best range was obtained, a simulation plot is presented.

In order to investigate the effect of the substrate type, thickness is fixed to 0.51 mm, and simulations have been repeated by using FR4 and RO4003C, which have a dielectric constant of 4.2 and 3.38, respectively. As seen in Fig. 8, the best absorption is obtained for the Magtrex 555 substrate. Furthermore, it is seen that the number of peak absorptions is related to the number of patches through Y-axis. FR4 also has good absorption over 14 GHz with more than 50% absorptivity. An increase in dielectric constant positively affects the absorptivity due to high capacitance.

The structural responses were thoroughly examined by analysing the electric field distributions across various frequencies. Figure 9(a) presents these distributions at specific frequencies, including 3 GHz, 4 GHz, 7 GHz, 10 GHz, 16 GHz, and 20 GHz. The intensity of the electric field is visually represented using a colour scale, where red indicates the highest intensity regions, while blue signifies the lowest, with intermediate shades depicting varying intensities. At 3 GHz, the electric field distribution displays multiple concentrated high-intensity areas, appearing in red and orange, whereas the low-intensity zones are represented in green and blue. This pattern is intricate with numerous localized regions dispersed across the broader sections of the metallic absorber layer. The distribution at 4 GHz resembles that of 3 GHz but exhibits slight

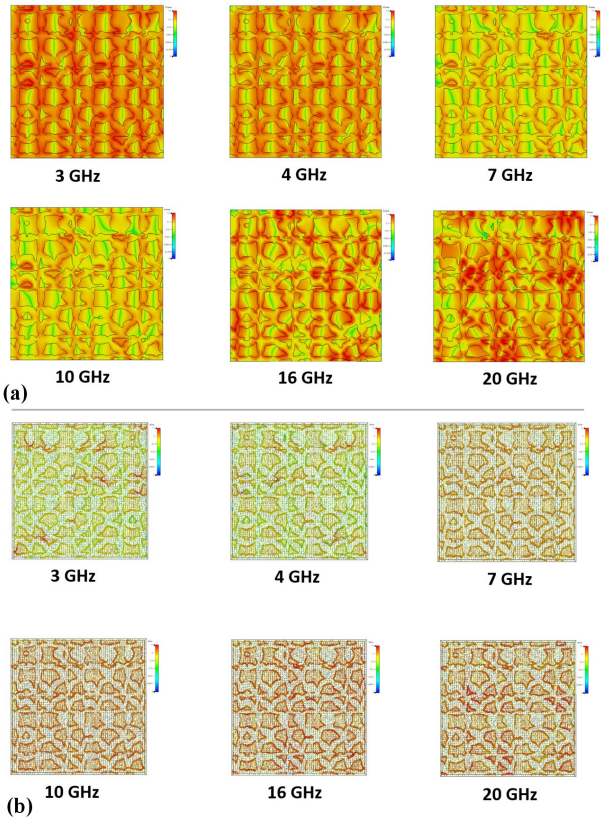

Fig. 9. (a) Electric field and (b) surface current distributions for resonant frequencies of 3 GHz, 4 GHz, 7 GHz, 10 GHz, 16 GHz, and 20 GHz.

differences in the arrangement of peak intensity areas. For 7 GHz and 10 GHz, the intensity is notably lower, which aligns with expectations. However, at 16 GHz and 20 GHz, the electric field exhibits stronger intensity with more pronounced high-energy regions, as indicated by an increased presence of red zones. The distribution of the electric field undergoes significant transformations as the frequency changes. At higher frequencies, the high-intensity regions become more localized, and the overall complexity of the field patterns increases. This behaviour highlights the intricate interaction between the electromagnetic waves and the surrounding medium, revealing a dynamic relationship influenced by frequency variations.

As a conclusion to the electric field distributions, these distributions are related to the resonant modes of the designed absorber structure, material properties, and specific configuration of the electromagnetic system being operated.

Figure 9(b) illustrates the surface current distributions of the proposed metamaterial absorber at various resonant frequencies (3 GHz, 4 GHz, 7 GHz, 10 GHz, 16 GHz, and 20 GHz). The distributions reveal how the current intensity changes across to the surface as frequency increases, providing insights into the absorber performance. At lower frequencies (3 GHz and 4 GHz), the surface currents are more uniformly distributed across larger regions of the structure. This indicates that longer wavelengths of low-frequency waves interact with broader portions of the chaotic patterns, leading to a widespread current flow across larger metallic areas. As the frequency increases to 7 GHz and 10 GHz, the surface currents become more localized and complex at certain regions exhibiting stronger current density. This reflects a more selective interaction between the electromagnetic waves and the chaotic structure, where only specific regions resonate at these mid-level frequencies. The surface current distributions at higher frequencies (16 GHz and 20 GHz) show significant localization in specific regions. This is primarily due to the shorter wavelengths of higher frequencies, which resonate more effectively with finer details of the chaotic pattern. The sharp concentration of currents near the edges of the structure indicates a stronger resonant characteristic, which contributes to improved electromagnetic absorption. The chaotic nature of design introduces irregularities and varying feature sizes, allowing for multiple resonances to occur over a broad frequency range, with the smaller features contributing to localized resonances at higher frequencies.

The complex interaction between the chaotic geometry and the electromagnetic waves obtains the observed current distributions for different frequencies. The Chen attractor-derived patterns create both large and small resonant features supporting broadband frequency absorption. Surface plasmon resonance significantly concentrates currents at higher frequencies, especially around edges and sharp features, resulting in hotspots that enhance absorption. These distributions align with the design objective to achieve efficient absorption across a wide bandwidth, with the chaotic pattern enabling multi-band functionality by interacting with the electromagnetic waves in a highly dynamic and complex manner.

As demonstrated in Fig. 10, the absorptivity of the system is exhibited across TE, TM, and TEM modes within the frequency range from 2 GHz to 20 GHz. Notably, the absorptivity values exceed 90% for all three modes. At 20 GHz, the absorptivity values in TE and TM modes demonstrate a decline, with a decrease rate in TE mode being considerably higher than in TM mode. Furthermore, within the 18.5–20 GHz frequency range, the absorptivity value in TE mode exhibits a decline ranging from 90% to 88.5%. The absorptivity value in TEM mode decreases to 90% in the 5–10 GHz range and varies between 95% and 97% in the 10–20 GHz range. It is evident that higher values are obtained compared to those observed in other modes. These results suggest that the structural configuration efficiently supports multiple modes with minimal variation, emphasizing its mode-agnostic performance and effectiveness across a wide frequency range.

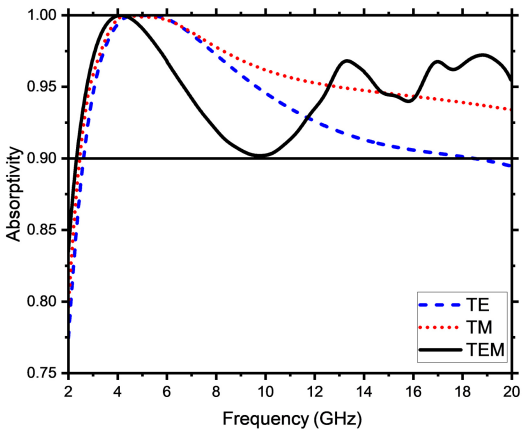

Fig. 10. Absorbtivity of a chaotic patterned microwave absorber for TE, TM, and TEM modes.

In order to explain that the metallic back plate serves as a reflective ground plane, conditions similar to a Salisbury screen were created. This approach highlights how it complements the chaotic mesh patterns to achieve broadband absorption. A set of simulation work, which is briefly given in Fig. 11(a) and Fig. 11(b), is presented. As is seen from Fig. 11, absorption decreased dramatically to 0.4 without a back plate. Another simulation was prepared to show the performance of the backplate by putting a mirror image of the front face to the back of the substrate, as depicted in the dashed line. This simulation shows that the metallic back plate is a crucial component, reflecting electromagnetic waves back into the absorber to enhance absorption efficiency.

Finally, a simulation was conducted to demonstrate the Salisbury screen effect on absorption by replacing the chaotic metamaterial on the front side with a resistive plate of 377 Ω/m. This allowed a direct comparison between the Salisbury screen and the chaotic metamaterial-based absorber. As shown in Fig. 11(b), the Salisbury screen achieves near-perfect absorption only within the frequency range of 2 GHz to 8 GHz. The spacer provides a quarter-wavelength condition for destructive interference between the incident and reflected waves, which minimizes the reflected energy and enhances absorption between 2 GHz and 8 GHz. Figures 11(a) and 11(b) show that the proposed chaotic-based metamaterial structure provides perfect absorption between 2 GHz and 20 GHz.

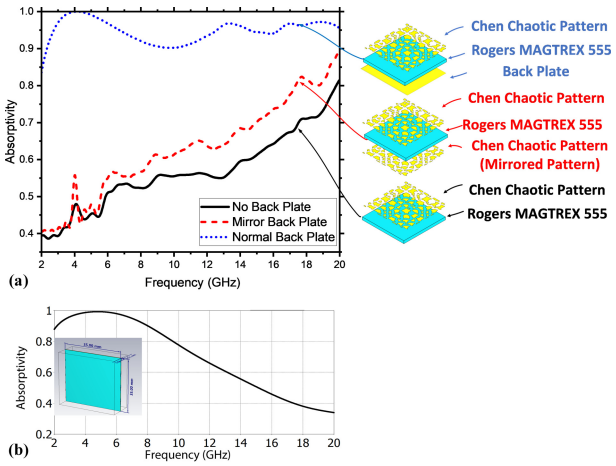

Fig. 11. (a) Absorption with no back plate, mirror back plat, and normal back plate; (b) absorption with resistive layer and metallic back plate.

4. Comparison with similar works

Future studies will focus on refining the metamaterial absorber design by investigating other chaotic systems like the Lorenz or Rossler attractors, which could provide new resonant features and offer enhanced absorption capabilities. By experimenting with these different chaotic dynamics, the authors aim to achieve improved broadband absorption and tailor the design for specific frequency ranges. Additionally, integrating adaptive materials into the absorber could enable tunability, allowing for real-time adjustment of the operating frequencies. This would expand the potential applications of the absorber in areas such as smart electromagnetic shielding, adaptive antennas, and stealth technologies.

Moreover, further work will aim to extend the absorption range to higher frequency domains, including millimetre-wave and terahertz frequencies, by scaling the chaotic patterns and refining the fabrication techniques. It will also be crucial to test the absorber performance under real-world conditions, considering factors such as temperature fluctuations, polarization, and varying incident angles. Experimental validation, complementing the numerical simulations, will be key to demonstrating the absorber practical applicability in advanced fields such as energy harvesting, wireless communications, and sensing technologies.

In conclusion, this study was evaluated in comparison with the existing research, as summarized in Table 1, which highlights the benefits of the proposed absorber design. Table 1 presents a comparative analysis of different microwave absorbers, outlining their absorption bandwidths, RCS reduction capabilities, substrate thicknesses, peak absorption values, and material compositions. The findings indicate that the proposed structure offers an exceptionally broad absorption range from 2 GHz to 20 GHz, surpassing many previously reported designs and demonstrating superior performance across various frequency ranges. Unlike conventional approaches, this design leverages a chaos-based methodology to achieve a full-bandwidth coverage within this range. Furthermore, the use of a thinner substrate enhances both the practicality and feasibility of the absorber, making it more suitable for real-world applications.

5. Conclusions

This study introduces a novel approach to the broadband metamaterial absorber design by integrating chaotic dynamics with substrate optimization. The use of the Chen attractor system enabled the creation of intricate, non-periodic patterns that significantly enhanced electromagnetic absorption across a wide frequency range (2 GHz to 20 GHz). These chaotic patterns provided multiple resonant features, ensuring broad and efficient wave absorption, surpassing traditional patterned absorbers in effectiveness.

A key factor in this performance was the selection of the Magtrex 555 substrate. Its frequency-dependent permittivity and permeability, combined with an optimal thickness of 0.51 mm, were crucial in maximizing absorption efficiency. The synergy between chaotic patterning and substrate properties resulted in absorption rates exceeding 90%, outperforming conventional materials like FR4 and RO4003C. This integration of the chaos theory with material selection represents a significant advancement in metamaterial design with promising applications in electromagnetic shielding, stealth technology, and energy harvesting.

Beyond demonstrating the value of chaotic systems in absorber design, this study highlights how randomness and determinism can be harmonized to inspire innovative engineering solutions. Rather than relying solely on chaotic randomness, the authors refined these patterns through a systematic and rational design process to optimize performance.

Future research could explore additional chaotic systems and further optimize substrate properties to extend absorption into higher frequency ranges. Additionally, incorporating advanced optimization techniques like machine learning or evolutionary algorithms could enhance

Table 1.
Comparative table of the proposed and similar work.

Ref.	Measured absorption bandwidth	Substrate thickness (mm)	Maximum absorption and peaks	Material information
[34]	6.16–41.63 GHz	$H = 2, 4, 6$ mm	−25 dB for 22.7 GHz	Metamaterial-based absorber
[35]	5–31 GHz	2 mm	50%–80% tunable absorption	Metasurface-based absorber
[36]	10.5–20.5 GHz	3 mm	Over 90%	Chaos-based metamaterial
[37]	1.61–4.45 GHz	0–2 mm	Over 90% absorption 99% for 2.01 GHz 95% for 4.12 GHz	Metamaterial and air combination.
[38]	5.56–12.99 GHz	6.6 mm	−20 dB for 8–12 GHz band	Rössler chaos metasurface; resistive top layer; dielectric substrate; back metal plate.
[39]	5.376–12.184 GHz	6 mm	−15 dB for 6.376–11.496 GHz band	Rössler chaos patterned metasurface; polyurethane foam plastic as substrate.
[40]	10–40 THz	900 nm	8 absorption points observed in a given band	Roger RT5870 material.
[41]	4.6–7.2 GHz	3.2 mm	Over 90% for 4.82–7.15 GHz band	Ultra-thin metamaterial; FR4 substrate with L-shaped copper patches.
[42]	3.95–8.02 GHz	4.2 mm	Over 90% absorption for 3.95–8.02 GHz band	Metamaterial copper film is separated by dielectric substrate FR4.
[43]	7.55–15.30 GHz	1.6 mm	Over 75%	Metamaterial-based absorber.
[44]	4.5–12 GHz	5.8 mm	Over 90% absorption for 4.5–12 GHz band	Metamaterial copper periodic structure substrate by PTFE material.
This study	2–20 GHz	0.51 mm	Over 90% absorption for 2.8–20 GHz band	Metamaterial Chen chaotic pattern over Rogers MAGTREX 555 substrate.

the design process by identifying even more effective configurations. Expanding this methodology to other material systems or multifunctional structures could unlock new possibilities in electromagnetic engineering.

Acknowledgements

This work was supported by "The Scientific and Technological Research Council of Turkey (TUBITAK)" with project no. 123F245.

References

[1] Abdulkarim, Y. I., Deng, L., Altıntaş, O., Ünal, E. & Karaaslan, M. Metamaterial absorber sensor design by incorporating swastika shaped resonator to determination of the liquid chemicals depending on electrical characteristics. *Phys. E Low Dimens. Syst. Nanostruct.* **114**, 113593 (2019). https://doi.org/10.1016/j.physe.2019.113593

[2] Almutairi, A. F. *et al*. A complementary split ring resonator based metamaterial with effective medium ratio for C-band microwave applications. *Results Phys.* **15**, 102675 (2019). https://doi.org/10.1016/j.rinp.2019.102675

[3] Prakash, D. & Gupta, N. Applications of metamaterial sensors: A review. *Int. J. Microw. Wirel. Technol.* **14**, 19–33 (2022). https://doi.org/10.1017/S1759078721000039

[4] Abdulsattar, R. K., Elwi, T. A. & Abdul Hassain, Z. A. A new microwave sensor based on the moore fractal structure to detect water content in crude oil. *Sensors* **21**, 7143 (2021). https://doi.org/10.3390/s21217143

[5] Abdulkarim, Y. I. *et al*. The detection of chemical materials with a metamaterial-based sensor incorporating oval wing resonators. *Electronics* **9**, 825 (2020). https://doi.org/10.3390/electronics9050825

[6] Njogu, P. M., Sanz-Izquierdo, B. & Parker, E. A. A liquid sensor based on frequency selective surfaces. *IEEE Trans. Antennas Propag.* **71**, 631–638 (2022). https://doi.org/10.1109/TAP.2022.3219540

[7] Abdulkarim, Y. I. *et al*. A review on metamaterial absorbers: Microwave to optical. *Front. Phys.* **10**, 893791 (2022). https://doi.org/10.3389/fphy.2022.893791

[8] Meenakshi, Saurav, P. & Kishor, K. Design and simulation of metamaterial under the THz frequency for short-range wireless communication and military purposes. *Mater. Today: Proc.* **62**, 3729–3733 (2022). https://doi.org/10.1016/j.matpr.2022.04.437

[9] Qiu, Y., Zhang, P., Li, Q., Zhang, Y. & Li, W. A perfect selective metamaterial absorber for high-temperature solar energy harvesting. *Sol. Energy* **230**, 1165–1174 (2021). https://doi.org/10.1016/j.solener.2021.11.034

[10] Bakır, M., Karaaslan, M., Unal, E., Akgol, O. & Sabah, C. Microwave metamaterial absorber for sensing applications. *Opto-Electron. Rev.* **25**, 318–325 (2017). https://doi.org/10.1016/j.opelre.2017.10.002

[11] Ramya, S. & Srinivasa Rao, I. An ultra-thin compact wideband metamaterial absorber. *Radioengineering* **27**, 364–372 (2018). https://doi.org/10.13164/re.2018.0364

[12] Meng, Q., Zheng, L., Chen, F., Zhang, H. & Yang, W. High-efficiency broadband perfect absorber based on a multilayered pyramid structure. *Phys. Scr.* **98**, 015811 (2022). https://doi.org/10.1088/1402-4896/aca72a

[13] Chikhi, N., Passarelli, A., Andreone, A. & Masullo, M. R. Pyramidal metamaterial absorber for mode damping in microwave resonant structures. *Sci. Rep.* **10**, 19352 (2020). https://doi.org/10.1038/s41598-020-76433-3

[14] Yu, P. *et al*. Broadband metamaterial absorbers. *Adv. Opt. Mater.* **7**, 1800995 (2019). https://doi.org/10.1002/adom.201800995

[15] Chen, W., Chen, R., Zhou, Y. & Ma, Y. Broadband metamaterial absorber with an in-band metasurface function. *Opt. Lett.* **44**, 1076–1079 (2019). https://doi.org/10.1364/OL.44.001076

[16] Yao, X. *et al*. Design of an ultra-broadband microwave metamaterial absorber based on multilayer structures. *Int. J. RF Microw. Comput.-Aided Eng.* **32**, e23222 (2022). https://doi.org/10.1002/mmce.23222

[17] Wang, B.-X., Xu, C., Duan, G., Xu, W. & Pi, F. Review of broadband metamaterial absorbers: from principles, design strategies, and tunable properties to functional applications. *Adv. Funct. Mater.* **33**, 2213818 (2023). https://doi.org/10.1002/adfm.202213818

[18] Shen, Y. *et al*. Transparent broadband metamaterial absorber enhanced by water-substrate incorporation. *Opt. Express* **26**, 15665–15674 (2018). https://doi.org/10.1364/OE.26.015665

[19] Nguyen, T. T. & Lim, S. Angle-and polarization-insensitive broadband metamaterial absorber using resistive fan-shaped resonators. *Appl. Phys. Lett.* **112**, 021605 (2018). https://doi.org/10.1063/1.5004211

[20] Zhang, Z. *et al*. Broadband metamaterial absorber for low-frequency microwave absorption in the S-band and C-band. *J. Magn. Magn. Mater.* **497**, 166075 (2020). https://doi.org/10.1016/j.jmmm.2019.166075

[21] Zhang, C. *et al*. Hybrid metamaterial absorber for ultra-low and dual-broadband absorption. *Opt. Express* **29**, 14078–14086 (2021). https://doi.org/10.1364/OE.423245

[22] Sayed, S. I., Mahmoud, K. R. & Mubarak, R. I. Design and optimization of broadband metamaterial absorber based on manganese for visible applications. *Sci. Rep.* **13**, 11937 (2023). https://doi.org/10.1038/s41598-023-38263-x

[23] Alavikia, B., Almoneef, T. S. & Ramahi, O. M. Wideband resonator arrays for electromagnetic energy harvesting and wireless power transfer. *Appl. Phys. Lett.* **107**, 243902 (2015). https://doi.org/10.1063/1.4937591

[24] Tu, J. The Design of Conformal and Chaotic Electromagnetic Stealth Metasurface for Arbitrary NURBS Curved Surfaces. in *2021 Global Symposium on Millimeter-Waves & Terahertz (GSMM)* 1–6 (IEEE, 2021). https://doi.org/10.1109/GSMM53250.2021.9511899

[25] Gros, J. B., del Hougne, P. & Lerosey, G. Tuning a regular cavity to wave chaos with metasurface-reconfigurable walls. *Phys. Rev. A* **101**, 061801 (2020). https://doi.org/10.1103/PhysRevA.101.061801

[26] Yuan, X. *et al*. Wideband high-absorption electromagnetic absorber with chaos patterned surface. *IEEE Antennas Wirel. Propag. Lett.* **18**, 197–201 (2018). https://doi.org/10.1109/LAWP.2018.2886049

[27] Chen, G. & Ueta, T. Yet another chaotic attractor. *Int. J. Bifurc. Chaos* **9**, 1465–1466 (1999). https://doi.org/10.1142/S0218127499001024

[28] Ramakrishna, S. A. Physics of negative refractive index materials. *Rep. Prog. Phys.* **68**, 449 (2005). https://doi.org/10.1088/0034-4885/68/2/R06

[29] Jiao, P., Mueller, J., Raney, J. R., Zheng, X. & Alavi, A. H. Mechanical metamaterials and beyond. *Nat. Commun.* **14**, 6004 (2023). https://doi.org/10.1038/s41467-023-41679-8

[30] Ong, K.-K., Shiah, A. & Musielak, Z. E. Fractal images of generalized Julia sets. *Fractals* **4**, 533–541 (1996). https://doi.org/10.1142/S0218348X96000649

[31] Alpigini, J. J. The evaluation and visualization of system performance in chaotic dynamical systems. *Inf. Sci.* **127**, 173–192 (2000). https://doi.org/10.1016/S0020-0255(00)00038-4

[32] Lee, J.-S. Digital image smoothing and the sigma filter. *CVGIP* **24**, 255–269 (1983). https://doi.org/10.1016/0734-189X(83)90047-6

[33] Nuñez-Perez, J. C., Adeyemi, V. A., Sandoval-Ibarra, Y., Perez-Pinal, F. J. & Tlelo-Cuautle, E. Maximizing the chaotic behavior of fractional order Chen system by evolutionary algorithms. *Mathematics* **9**, 1194 (2021). https://doi.org/10.3390/math9111194

[34] Su, J. *et al*. Ultrawideband radar cross-section reduction by a metasurface based on defect lattices and multiwave destructive interference. *Phys. Rev. Appl.* **11**, 044088 (2019). https://doi.org/10.1103/PhysRevApplied.11.044088

[35] Xing, B.-B., Liu, Z.-G., Lu, W.-B., Chen, H. & Zhang, Q.-D. Wideband microwave absorber with dynamically tunable absorption based on graphene and random metasurface. *IEEE Antennas Wirel. Propag. Lett.* **18**, 2602–2606 (2019). https://doi.org/10.1109/LAWP.2019.2944966

[36] Wang, H. *et al*. Chaos-based coding metasurface for radar cross-section reduction. *J. Phys. D: Appl. Phys.* **52**, 405304 (2019). https://doi.org/10.1088/1361-6463/ab2dc6

[37] Ma, X., Tian, F., Li, X., Guo, L. & Huang, X. Broadband with enhanced oblique incidence metamaterial absorber. *Mater. Res. Express* **7**, 095803 (2020). https://doi.org/10.1088/2053-1591/abba9e

[38] Yuan, X. *et al*. Wideband high-absorption electromagnetic absorber with chaos patterned surface. *IEEE Antennas Wirel. Propag. Lett.* **18**, 197–201 (2018). https://doi.org/10.1109/LAWP.2018.2886049

[39] Zhang, R., Ding, F., Yuan, X. & Chen, M. Influence of spatial correlation function on characteristics of wideband electromagnetic wave absorbers with chaotic surface. *Chin. Phys. Lett.* **39**, 094101 (2022). https://doi.org/10.1088/0256-307X/39/9/094101

[40] Köksal, A. S. & Ünal, S. Multiband absorber design and optimization with Lorenz chaotic attractor. *Phys. Scr.* **98**, 115522 (2023). https://doi.org/10.1088/1402-4896/ad008e

[41] Bhattacharyya, S., Ghosh, S., Chaurasiya, D. & Srivastava, K. V. A Broadband Wide Angle Metamaterial Absorber for Defense Applications. in *2014 IEEE International Microwave and RF Conference (IMaRC)* 33–36 (IEEE, 2014). https://doi.org/10.1109/IMaRC.2014.7038964

[42] Tuan, T. S., Lam, V. D. & Hoa, N. T. Q. Simple design of a copolarization wideband metamaterial absorber for C-band applications. *J. Electron. Mater.* **48**, 5018–5027 (2019). https://doi.org/10.1007/s11664-019-07301-8

[43] Sood, D. & Tripathi, C. C. Broadband ultrathin low-profile metamaterial microwave absorber. *Appl. Phys. A* **122**, 332 (2016). https://doi.org/10.1007/s00339-016-9884-2

[44] Xu, Y., Zhang, B., Duan, J. & Tian, Y. Design of Broadband Metamaterial Absorber for C Band and X Band. in *2018 IEEE International Conference on Computer and Communication Engineering Technology (CCET)* 159–163 (2018).